INVESTIGATION INTO THE CAPABILITIES AND CHARACTERISTICS OF TOMOGRAPHIC PARTICLE IMAGE VELOCIMETRY MEASUREMENT TECHNIQUES

by

Tucker Bisel

A thesis submitted to the faculty of
The University of North Carolina at Charlotte
in partial fulfillment of the requirements
for the degree of Master of Science in
Mechanical Engineering

Charlotte

2018

Approved by:

_____

Dr. Peter Tkacik

_____

Dr. Navid Goudarzi

_____

Dr. Samuel Hellman

ABSTRACT

TUCKER BISEL. Investigation into the capabilities and characteristics of tomographic particle image velocimetry measurement techniques. (Under the direction of DR. PETER TKACIK)

Literature describing measurement results obtained using tomographic particle image velocimetry (TomoPIV) systems has become increasingly common, but details on the processes used to obtain those results and reasons for selecting specified analysis settings are not often explained. In this thesis, an overview is given of techniques and methodologies found to be useful when conducting TomoPIV measurements using an asymmetric four-camera system, including image pre-processing techniques and methods of improving analysis settings. Effective image pre-processing techniques include background subtraction for removing static background noise and improving signal-to-noise ratios and a customized filter that easily and reliably increases voxel reconstruction speed and reduces memory requirements. The custom filter acts to concentrate light intensity around particle locations while muting background pixel intensities. The effects on final measurement results are observed for voxel reconstruction and 3D least squares matching (LSM) settings, including relaxation number, reconstruction iterations, and interrogation volume size. The effects of surface reflections of laser light on TomoPIV results are also investigated by comparing measurement results of a cubic bluff body painted first with a flat white aerosol paint, and second with an airbrushed Rhodamine 6G fluorescent paint. Fluoresced light is blocked by bandpass filters, resulting in minimal reflections from the Rhodamine 6G paint and no observed impact on measurement results. White paint results in intense surface reflections and increased image noise, preventing reliable recognition of distant particles. Comparison of averaged 3D vector map results for both coatings reveals that allowable measurement depth decreases as surface reflection intensity increases.

ACKNOWLEDGEMENTS

I would like to express my gratitude for continued resources and support from my advisor, Dr. Peter Tkacik, as well as the members of my advisory committee, Dr. Navid Goudarzi and Dr. Samuel Hellman. This research was supported by funding from the Office of Naval Research (ONR N00014-15-1-0020), as well equipment and technical assistance from Dantec Dynamics. I would finally like to thank the University of North Carolina at Charlotte Department of Mechanical Engineering for financial support through teaching assistantships.

TABLE OF CONTENTS

LIST OF FIGURES vi

LIST OF ABBREVIATIONS ix

CHAPTER 1: INTRODUCTION 1

CHAPTER 2: EQUIPMENT AND METHODS 4

CHAPTER 3: RESULTS AND DISCUSSION 7

3.1. IMAGE PRE-PROCESSING 7

3.2. VOXEL RECONSTRUCTION 13

3.3. 3D LEAST SQUARES MATCHING 18

3.4. EFFECTS OF REFLECTION MITIGATION 24

CHAPTER 4: CONCLUSIONS 32

REFERENCES 36

APPENDIX A: VOXEL RECONSTRUCTION ITERATION AND RELAXATION COMPARISONS 38

LIST OF FIGURES

FIGURE 2.1: Overhead view of water channel experimental setup (left). Camera configuration (right). 4

FIGURE 3.1: View of particles after performing image minimum background subtraction. Insert: typical pixel gray value distribution; many non-zero values remaining. 7

FIGURE 3.2: View of particles after performing image minimum background subtraction, then applying a custom filter described in Figure 3.4. Insert: typical pixel gray value distribution; increased particle intensity, and many gray values reduced to zero. 8

FIGURE 3.3: View of particles after performing image minimum background subtraction, then applying thresholding process. Insert: typical pixel gray value distribution; many gray values reduced to zero. 9

FIGURE 3.4: A customized filter designed to concentrate light at particle locations. 10

FIGURE 3.5: Left: too few SMART iterations for a given relaxation number displays gaps in measurement results (regions of no or very slow motion); vector map produced using 0.1 relaxation, 5 iterations. Right: an adequate number of iterations fills in the measurement gaps; vector map produced using 0.1 relaxation, 40 iterations. 15

FIGURE 3.6: Vector map created using an insufficiently large IV size, producing noisy measurement results (used IV size of 51x51x51 voxels; recommended minimum IV size was 71x71x71 voxels). 18

FIGURE 3.7: Vector map created using a sufficiently large IV size, producing relatively smooth measurement results (used IV size of 75x75x75 voxels; recommended minimum IV size was 71x71x71 voxels). 20

FIGURE 3.8: LSM measurement results based on an insufficiently large time step (resultant particle displacements of 1 to 2 pixels). Velocity vectors extend beyond 50 mm illumination depth (region between planes). 21

FIGURE 3.9: LSM measurement results based on a sufficiently large time step (resultant particle displacements of 5 to 6 pixels). Velocity vectors generally confined to 50 mm illumination depth (region between planes). 22

FIGURE 3.10: LSM measurement results based on the same time step as Figure 3.9. Image pre-processing utilized only thresholding, no custom filter. Vectors once again extend beyond 50 mm illumination depth (region between planes). 23

FIGURE 3.11: Background subtraction sequence for camera 1 (centerline) view of white model: raw image (a), image min (b), background subtraction (c). 25

FIGURE 3.12: Background subtraction sequence for camera 1 (centerline) view of Rhodamine 6G model: raw image (a), image min (b), background subtraction (c). 25

FIGURE 3.13: Background subtraction sequence for camera 4 (45 degree offset) view of white model: raw image (a), image min (b), background subtraction (c). 26

FIGURE 3.14: Background subtraction sequence for camera 4 (45 degree offset) view of Rhodamine 6G model: raw image (a), image min (b), background subtraction (c). 26

FIGURE 3.15: Average of 125 vector maps for the white paint model (angled front view). 27

FIGURE 3.16: Average of 125 vector maps for the white paint model (upstream view). 28

FIGURE 3.17: Average of 125 vector maps for the Rhodamine 6G paint model (angled front view). 29

FIGURE 3.18: Average of 125 vector maps for the Rhodamine 6G paint model (upstream view). 30

FIGURE A.1: Vector maps created using 0.001 relaxation from data with a strong signal-to-noise ratio. Left: 2 SMART iterations. Right: 30 SMART iterations. Bottom: Difference between results (left subtracted from right). 38

FIGURE A.2: Vector maps created using 0.001 relaxation from data with a relatively weak signal-to-noise ratio. Left: 5 SMART iterations. Right: 40 SMART iterations. Bottom: Difference between results (left subtracted from right). 39

FIGURE A.3: Left: vector map created from the same data as Figure A.1 (0.001 relaxation), using 2 SMART iterations and 0.01 relaxation. Right: difference between 0.01 and 0.001 relaxation results. 39

FIGURE A.4: Left: vector map created from the same data as Figure A.1 (0.001 relaxation), using 2 SMART iterations and 0.1 relaxation. Right: difference between 0.1 and 0.001 relaxation results. 40

FIGURE A.5: Left: vector map created from the same data as Figure A.1 (0.001 relaxation), using 2 SMART iterations and 0.95 relaxation. Right: difference between 0.95 and 0.001 relaxation results. 40

LIST OF ABBREVIATIONS

IV	Interrogation Volume
LSM	3D Least Squares Matching
PIV	Particle Image Velocimetry
SMART	Simultaneously Multiplicative Algebraic Reconstruction Technique
TomoPIV	Tomographic Particle Image Velocimetry

CHAPTER 1: INTRODUCTION

Understanding flow phenomena often requires analysis of boundary layer characteristics and near-body interactions. Any analysis method used to measure these flow regions must be non-intrusive since any intrusion will disrupt the flow characteristics [1]. PIV systems are non-intrusive measurement tools and have been used since 1984 [2]. Adrian [3] provides a detailed report of the development of PIV systems from 1984 to 2005. PIV systems use thin light sheets, typically from a high-power laser, to illuminate neutrally buoyant seed particles. Early PIV systems typically used a single camera to record particle positions, with short time steps between images. Changes in particle positions are correlated to extract velocity data from flow regions of interest. This approach is limited to two-dimensional measurement profiles, while thorough understanding of flow characteristics requires a three-dimensional (3D) measurement profile. Toward this end, advances have been made in PIV measurement systems, with dual-plane stereoscopic PIV allowing limited measurement of 3D velocity gradients. Tomographic PIV (TomoPIV), introduced in Elsinga et al. [4], uses three or more cameras positioned at different angles to image a 3D flow region typically illuminated by a volumetrically expanded laser source, rather than the thin light sheets used previously. The images from all camera views are correlated to reconstruct seed particle locations within the illuminated volume, producing a 3D (volumetric) voxel space. Velocity profiles can then be extracted from observed changes in particle location, resulting in a complete volumetric flow measurement profile [5]. The work presented in this thesis utilizes an asymmetric four-camera TomoPIV system.

Much of the available literature concerning TomoPIV typically either describes novel techniques aimed at improving analysis speed or accuracy, or presents TomoPIV

experimental flow measurements without giving detailed explanations of the methods used to obtain the results. When details are given, they are typically limited to measurement parameters such as voxel space resolution and vector map size and vector density. This neglects to mention the settings chosen for the intermediate measurement processes used in the commonly-available commercial TomoPIV measurement platforms (DynamicStudio by Dantec Dynamics, DaVis by LaVision, etc.). Even if the settings are specified, there is typically no explanation given for why or how those settings were determined to be appropriate. One of the goals of this thesis is to provide explanations of how various TomoPIV steps and settings impact final measurement results (specifically using the DynamicStudio 6.1 platform), as well as provide a sequence of simple-to-implement image pre-processing steps that are found to reliably improve TomoPIV measurement capabilities. This thesis should therefore provide quick guidance on the salient settings for TomoPIV analysis techniques, particularly those used in the DynamicStudio measurement platform, including Simultaneously Multiplicative Algebraic Reconstruction Technique (SMART) voxel reconstruction and 3D Least Squares Matching (LSM). Those unfamiliar with TomoPIV measurement techniques should be able to use these explanations first to roughly determine which measurement settings are appropriate for a given dataset, and second to refine the settings after examining preliminary measurement results.

Measurement results are affected not only by the settings chosen during TomoPIV analysis, but also, for obvious reasons, by the quality of raw measurement images. As noted in Bisel et al. [1], despite PIV systems being non-intrusive by nature, PIV resolution close to solid surfaces has generally been found to be very low due to surface reflections. To improve resolution, one strives to reduce image noise by avoiding as much reflected and scattered light as possible. Due to the high intensity light sources required to illuminate seed particles, surface reflections are common concerns for PIV measurements and are often identified as flares. The consequences of these flares may

include overexposure in near-surface regions, camera sensor damage, and skewing of results [6]. Surface reflections can compromise PIV measurements near the boundary regions as increased background noise intensity reduces seed particle signal-to-noise ratios. Hence, it is necessary to reduce surface reflections within the experimental setup [1]. A variety of works have described methods to reduce surface reflections during PIV measurements ([7, 8, 9, 10, 11]), but the observable effects of surface reflections on PIV measurements are generally neglected. This thesis will present measurement results that exhibit characteristic impacts of strong surface reflections on TomoPIV measurement capabilities.

In summary, this thesis intends to explore techniques used during TomoPIV analysis (conducted using the DynamicStudio 6.1 TomoPIV measurement platform) and explain how measurement settings affect final results, including characteristics indicating poor measurement results and strategies to improve the results. The necessity of reflection mitigation techniques for TomoPIV analysis will also be established via examination of TomoPIV results under conditions of strong surface reflections. The important TomoPIV measurement steps outlined in this thesis include image pre-processing, SMART voxel reconstruction parameters, and 3D LSM parameters. Image pre-processing techniques focus on removing image noise to increase analysis speeds and reduce computer memory requirements. Voxel reconstruction recreates the 3D spatial locations of particles in the measurement images. 3D LSM calculates velocity vectors based on changes in particle locations between two sequential reconstructed voxel spaces. The user-defined parameters for voxel reconstruction and LSM impact the quality of TomoPIV measurement results, but it can be difficult to determine the impact of a single setting. The observations made in this thesis should serve as a guide for recognizing characteristic signs of measurement inaccuracies and provide assistance in determining how to modify measurement parameters in order to improve results.

CHAPTER 2: EQUIPMENT AND METHODS

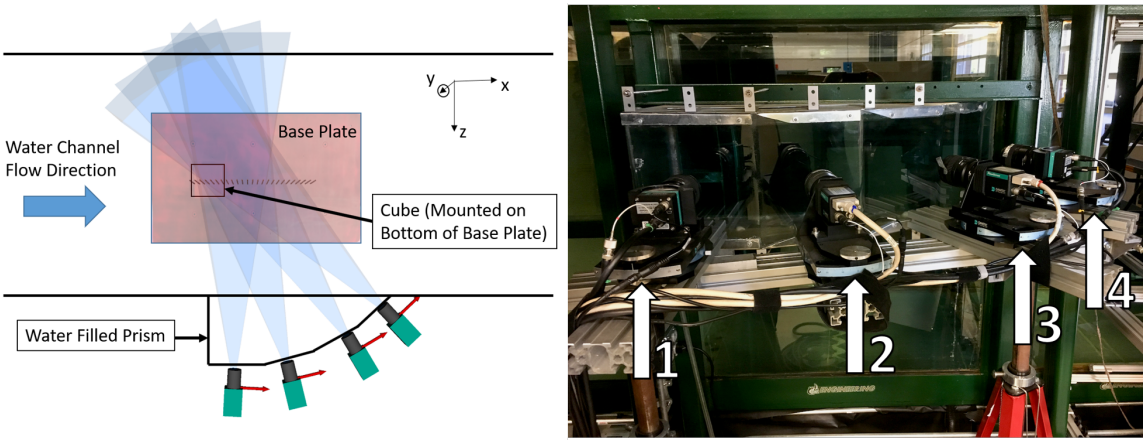

Figure 2.1: Overhead view of water channel experimental setup (left). Camera configuration (right).

TomoPIV measurement runs were conducted in a closed-loop water channel located at the University of North Carolina at Charlotte. The measurements utilized an asymmetric four-camera system described by Fleischhauer et al. [12]. The system consisted of four Flowsense EO 4M dual-frame CCD cameras with image resolutions of 2048 x 2048 pixels, and a DualPower dual cavity 532 nm Nd:YAG laser capable of outputting 200 mJ pulses with a pulse width of 4 nanoseconds. The laser pulses were expanded using 5:1 thickness-to-width volumetric optics from Dantec Dynamics. The laser illuminated the 1 m^3 test section from below through the glass floor of the water channel. The cameras were fitted with 60 mm lenses as well as narrow-band 532 nm optical bandpass filters. The camera configuration is seen in Figure 2.1, with the first camera positioned normal to the side of the water channel and subsequent cameras offset from the normal by 15, 30, and 45 degrees. A water-filled prism tank with angled faces matching the camera offset angles was fitted to the glass side of

the water channel. The prism faces are normal to the respective camera's viewing axis to minimize refractive errors associated with imaging an angled surface. The measurements focused on turbulent flow around a 76.2 mm cubic bluff body mounted to a flat plate. The plate was lowered into the test section with the bluff body facing downward.

The TomoPIV system required calibration to determine spatial positions in the measurement volume. The calibration images were acquired for each measurement run using a 450 x 450 mm dotted calibration target across a calibration depth of +/- 50 mm. A precision traverse was used to move the calibration target in increments of 5 mm, with a total of 21 calibration images captured per camera. To minimize vibration errors, the calibration target was allowed to settle for 10 seconds before capturing images at each position. A 3rd order polynomial calibration was conducted for each measurement run, resulting in an overall average re-projection error of 0.310 pixels. The re-projection error for each individual camera never exceeded 0.4, the maximum acceptable error specified by Elsinga et al. [4].

The bluff body model and flat plate were typically coated with a fluorescent Rhodamine 6G paint (from Flow Visualization Components, dr.gindele-fischer-nauwerck GBR) [13] in order to minimize surface reflections. The Rhodamine paint fluoresces orange when exposed to the green 532 nm laser, shifting the spectrum of reflected light to approximately 625 nm. The shifted light is then filtered out by the optical bandpass filters attached to the cameras. Multiple coats of Rhodamine paint were applied via airbrush, after which coverage was inspected visually using a hand-held 532 nm laser. A measurement run was also attempted without using fluorescent paint to reduce surface reflections. For that run the model was coated with a flat white aerosol paint (STRUST+SSPR FLAT WHITE) [14].

The water channel was seeded using neutrally-buoyant 50 μm polyamide spheres. The seeding density was varied over multiple measurement runs by adding seed par-

ticles to the channel, with seeding densities ranging from 0.005 to 0.035 particles per pixel. For all measurement runs, doubleframe image pairs were acquired at a rate of 5 Hz for up to 25 seconds, resulting in a maximum of 125 image pairs per run.

Image acquisition and tomographic analysis were performed using Dantec Dynamic's DynamicStudio 6.1 measurement platform. Analysis typically involved preprocessing of images, SMART voxel reconstruction, and 3D LSM. The reconstructed volume measured 200 x 140 x 100 mm with various voxel resolutions, typically 0.125 or 0.11 mm/voxel. Other SMART voxel reconstruction settings were varied for optimal results, with SMART iterations and relaxation numbers respectively varying from 30 and 0.2 for noisy measurement data, to 5 and 0.1 for data with strong signal-to-noise ratios. The LSM technique typically utilized Interrogation Volumes (IV) of 91 x 91 x 91 voxels for low seeding density measurements, and as low as 51 x 51 x 51 voxels for higher seeding density measurements. The typical IV step size was 30 voxels in all 3 directions, resulting in roughly 30,000 to 45,000 vectors per map depending on IV size and voxel resolution.

CHAPTER 3: RESULTS AND DISCUSSION

3.1 IMAGE PRE-PROCESSING

Image pre-processing is critical to making TomoPIV measurements feasible resource-wise. Pre-processing steps are necessary to remove noise from measurement images not only to improve accuracy, but also greatly reduce computer memory requirements during voxel reconstruction. Herein are presented image pre-processing methods found to be useful when conducting TomoPIV measurements.

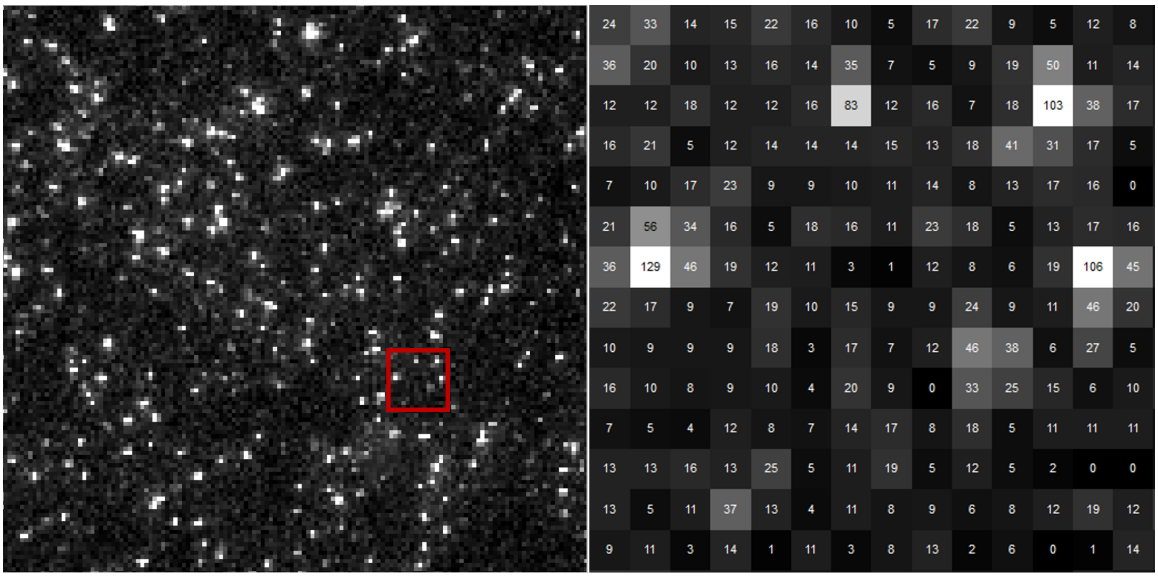

Figure 3.1: View of particles after performing image minimum background subtraction. Insert: typical pixel gray value distribution; many non-zero values remaining.

Background Subtraction: First, an image minimum background subtraction can be performed to remove background noise from a set of images. This function is available as a predefined analysis sequence in DynamicStudio, wherein an image minimum is calculated by finding the minimum intensity value (gray value) seen in an image set for each pixel coordinate. This image minimum (image min) represents an estimate

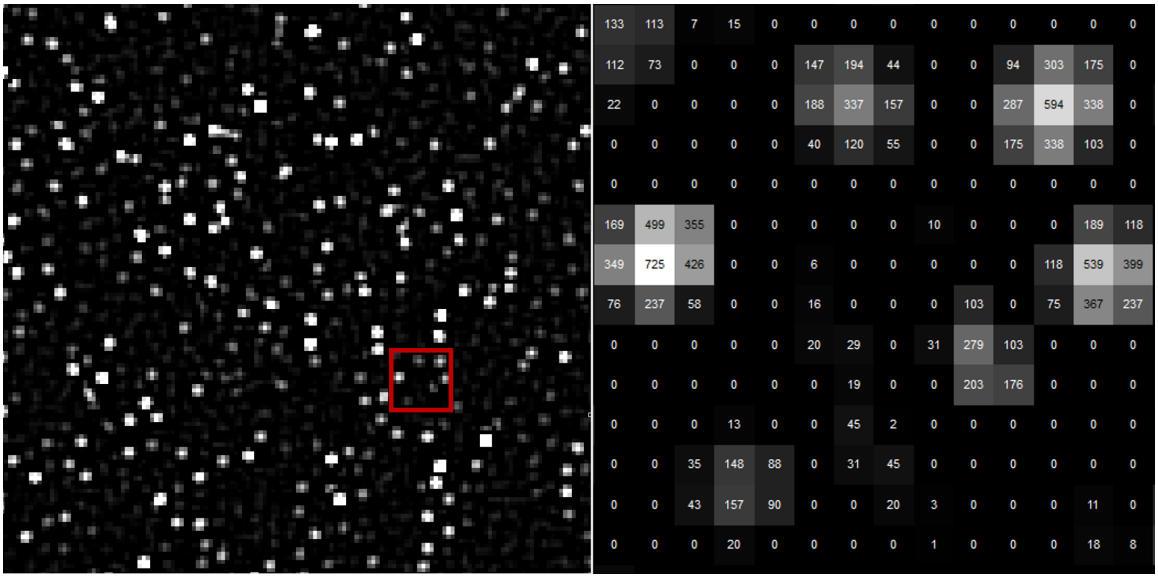

Figure 3.2: View of particles after performing image minimum background subtraction, then applying a custom filter described in Figure 3.4. Insert: typical pixel gray value distribution; increased particle intensity, and many gray values reduced to zero.

of the background noise present in the image set, and is most easily seen in Figures 3.12b and 3.14b. The gray values from the image min are then subtracted from every image in the parent image set to ostensibly remove all background noise, as seen in Figures 3.12c and 3.14c. Figure 3.1 shows a detailed view of a region of particles following a background subtraction, along with a sample gray value distribution to show the difference in intensity between seed particles and the background. The same region is shown following subsequent processing steps in Figures 3.2 and 3.3.

Custom Filter: A background subtraction improves signal-to-noise ratios, but generally some low-level gray values remain in most pixels, as seen in Figure 3.1. Every non-zero gray value increases the time and memory required for voxel reconstruction, so efforts must made to remove as many gray values as possible. A specially customized filter (Figure 3.4) has proven useful for this purpose. After background subtraction, the specified custom filter was applied to concentrate light at particle locations. This amplifies particle brightness and, more significantly, removes light from the surrounding background, as seen in the insert view of Figure 3.2. The pixels

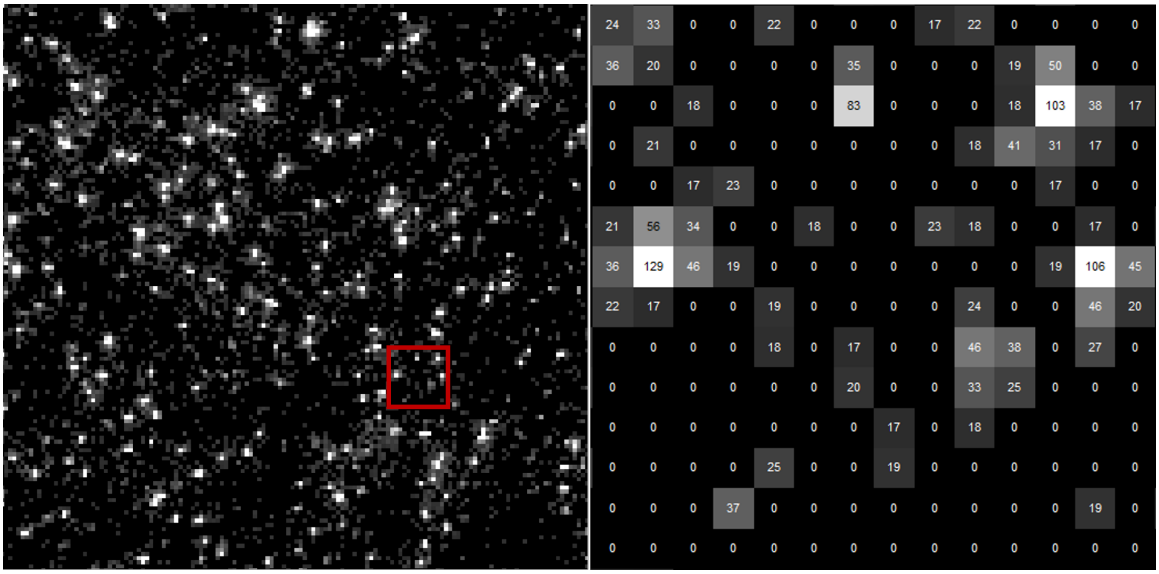

Figure 3.3: View of particles after performing image minimum background subtraction, then applying thresholding process. Insert: typical pixel gray value distribution; many gray values reduced to zero.

not representing particle locations generally have all light intensity removed, giving many pixels a gray value of zero. Every pixel with a non-zero gray value increases the computer memory required during SMART voxel reconstruction, so using the custom filter greatly speeds up voxel creation and reduces memory requirements, which is critical for reconstructing large volumes.

The custom filter shown in Figure 3.4 may be modified as desired, such as by changing the filter kernel size or increasing the filter divisor, but it should be noted that the filter must always use integer values, not floating point values. Using floating point filter values allows pixel gray values to become negative, producing undesirable results. Using integer filter values limits the minimum pixel gray value to zero.

The filter kernel size may require modification depending on the average particle spacing in the data that is to be filtered. When the custom filter is centered on a particle, ideally there should not be any other particles within the filter area. The filter kernel size should therefore be limited to twice the average particle spacing for any given image. DynamicStudio allows measurement of average particle spacing using

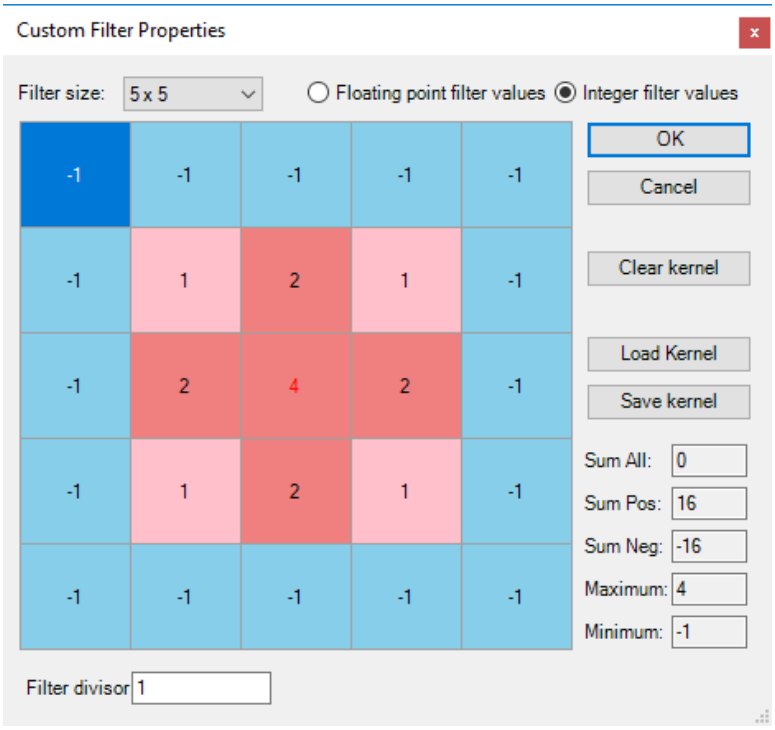

Figure 3.4: A customized filter designed to concentrate light at particle locations.

a built-in particle density measurement tool. The custom filter in Figure 3.4 uses a kernel size of 5 x 5 pixels, and may be used for average particle spacings as low as 3 pixels. Note that it is not a requirement to increase the kernel size to the maximum allowed for a given particle spacing; the 5 x 5 custom filter was successfully applied for average particle spacings ranging from 16.2 down to 5.8 pixels (for reference, the average particle spacing in Figure 3.1 is approximately 8.9 pixels).

A filter divisor may be used to reduce the magnitude of pixel gray values resulting from the custom filter. If applied, the filter divisor typically matches the central value of the filter kernel (4 in the case of the filter described in Figure 3.4). A filter divisor is useful when particles are already bright before the custom filter is applied. Without a filter divisor, the custom filter may amplify a significant number of pixel gray values beyond the maximum allowed value (4095 for the 12-bit pixel depth utilized in the experimental setup for this thesis). Any gray value exceeding the maximum is

clamped down to the maximum value, altering the light intensity distribution in the image and resulting in some signal strength loss.

Thresholding: Applying a threshold is another method used to mute pixel gray values to zero, and was typically used after the custom filter since some low-intensity gray values typically remained after applying the filter. These low-intensity gray values were easily removed using thresholding. Thresholding can be used to mute all pixel intensities below a specified value to zero, potentially allowing a majority of background noise to be muted to zero without using the custom filter. However, this is only possible for images with strong signal-to-noise ratios. If particle intensities are too low, it is difficult to remove large amounts of background noise without erasing low-intensity particles as well. Thresholding after applying the custom filter proves to be simpler and more reliably implemented than purely using thresholding. Pure thresholding without applying the custom filter requires careful inspection of noise levels, which may vary between the two frames in an image pair, across different cameras, and over the course of a measurement run. The custom filter consistently removes gray values regardless of noise level or local pixel intensity distributions, and can therefore be easily applied to multiple datasets. Particle intensities are also amplified and easily distinguished from remaining low-level background noise. The large difference between the background noise and the amplified particle intensities allows for simple application of thresholding following the custom filter, since each image set does not need careful inspection to determine a threshold level that will remove noise without removing particles. Following application of the custom filter, a general-purpose threshold of 30 was typically applied for all datasets.

Impact Of Light Intensity On Pre-Processing Ability: Analyses were attempted without using the custom filter in order to observe possible changes in measurement results. For this thesis, measurements were taken using two different light intensities. For one set of high light intensity measurement runs, the laser source was expanded to

the maximum allowed depth for the 5:1 volumetric optics, resulting in an illumination depth of roughly 50 mm. This produced images with sharply defined seed particles over the entire illumination depth and a maximum signal-to-noise ratio of roughly 20 after background subtraction. For one such measurement run, TomoPIV analysis was attempted using only a background subtraction and thresholding for image pre-processing, leaving out the custom filter. The threshold values were carefully chosen for each camera view to ensure adequate noise removal without compromising particle integrity. The number of pixel gray values reduced to zero using this method was comparable to that achieved during typical measurement runs using both the custom filter and thresholding, with roughly 3 million out of 4 million gray values reduced to zero. Figure 3.3 shows the gray value distribution that resulted from the thresholding process (threshold set to 17 for this camera view). The voxel reconstruction and LSM analysis times were also comparable to the times required for analyses that utilized the custom filter. The vector results for this analysis (Figure 3.10) appear similar to the results obtained when the custom filter was used (Figure 3.9) when considering only the region inside the 50 mm illumination depth. Outside this depth, no seed particles should be visible, and therefore no motion should be observed. However, the threshold-only results displayed motion vectors outside the illumination depth, while the custom filter results did not. This is a problem characteristic of measurement runs that use too small of time steps between image frames, resulting in small particle displacements. Section 3.3 describes the characteristics and potential causes of this problem in greater detail.

For a second set of measurement runs, the light intensity decreased as the illumination depth was expanded from 50 mm to roughly 100 mm. Seed particle intensity values were therefore reduced overall, with the particles most distant from the cameras having the weakest intensity. For these low light intensity runs it was found to be impossible to use thresholding to achieve results comparable in speed to the re-

sults attained by a combination of custom filter and thresholding. When attempting to remove a number of gray values comparable with the custom filter results, the required threshold levels were high enough to also remove a significant number of particles in addition to the background noise. At those threshold levels, voxel reconstruction and LSM analysis consistently produced few or no velocity vectors upon completion of analysis. When threshold levels were reduced sufficiently to produce adequate vector map results, the number of gray values removed was a fraction of the number removed using the combination of custom filter and thresholding. The voxel reconstructions (roughly 1600 x 1100 x 800 voxels) also required roughly 4 hours to complete, compared to roughly 15 minutes when using the custom filter. It is therefore quite clear that the custom filter produces results overall superior to those achieved purely through thresholding techniques. The custom filter, or a filter of similar design, is also indispensable for increasing analysis speed of datasets with weak signal-to-noise ratios.

Image Masking: Applying an image mask is the final step used to mute unwanted pixel intensities and thereby reduce memory requirements and increase speed during voxel reconstruction. The shape of the mask is defined to black out any image regions that should not contain particles. Masking is effectively employed when a model must be placed inside the illuminated measurement volume and the removal of the model body is desired in the measurement images.

3.2 VOXEL RECONSTRUCTION

Voxel reconstruction involves correlating particle positions across multiple camera angles to determine the 3D location of all seed particles in a calibrated measurement volume. The SMART voxel reconstruction method available in DynamicStudio has several user-defined settings that affect the speed and accuracy of the reconstruction. This section will detail the observed effects that particular settings have on final TomoPIV measurements, including voxel size, relaxation, and number of SMART

iterations.

Voxel Size: The resolution of a reconstructed voxel space is determined by the chosen voxel size. The voxel size should be close to the size represented by one pixel length in a set of images. DynamicStudio automatically suggests a voxel size based on the calibration performed for the measurement run. It was found not to be possible to significantly decrease the voxel size from the suggested size. The suggested voxel size for the described four camera setup was 0.106 mm/voxel. Attempted voxel reconstructions consistently resulted in errors when using voxel sizes below 0.098 mm/voxel. It was found to be possible, and sometimes preferable, to use a slightly larger than suggested voxel size. Using a larger voxel size reduces the number of voxels required to reconstruct a given volume, thereby reducing the required computer memory. This is helpful when reconstructing large voxel spaces with a limited amount of memory available. Increasing the voxel size to 0.125 mm/voxel produced satisfactory measurement results, and in some instances produced results superior to those obtained using 0.11 mm/voxel, despite 0.11 being closer to the suggested voxel size. Further increasing the voxel size to 0.15 mm/voxel resulted in significant information loss during voxel reconstruction and poor measurement results from 3D LSM, as should be expected from the loss in resolution.

Relaxation: The relaxation parameter was observed to relate directly with the number of particles recognized as valid during voxel reconstruction. According to the DynamicStudio user manual [15], the allowable range of the relaxation parameter is between 0 and 1, with a typical value of 0.1. Smaller relaxation numbers require more SMART iterations to produce noticeable changes in measurement results. A very small relaxation number permits very little change to occur between reconstruction iterations, since particle recognition constraints are "relaxed" by only a small amount every iteration. This can be observed in Figures A.1 and A.2, in which measurement results change very little for a relaxation number of 0.001 even after roughly 30 ad-

ditional iterations are added. Smaller relaxation numbers were observed to result in overall smoother vector maps following voxel reconstruction and LSM, as can be seen by comparing Figures A.3 and A.5. The smoother vector maps contained fewer vectors that pointed in obviously incorrect directions, as compared to the rougher vector maps produced using larger relaxation numbers. Vector maps containing many gaps in measurement results was determined to be a sign of too few SMART iterations used for a given relaxation number (Figure 3.5, left). The measurement gaps take the form of regions containing unreasonably small velocity vectors compared to the surrounding velocities. Depending on the visualization method, these regions may appear to contain no velocity vectors at all due to the extremely small vector sizes. Increasing the number of iterations fills in the measurement gaps, while also potentially increasing the number of large, inaccurate vectors. It is possible to filter out these large vectors using a range validation during post processing.

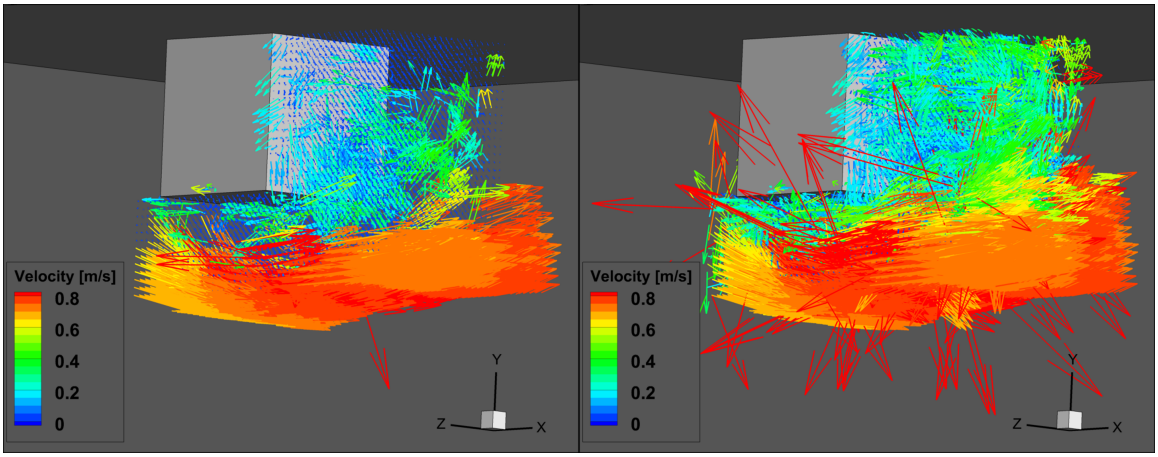

Figure 3.5: Left: too few SMART iterations for a given relaxation number displays gaps in measurement results (regions of no or very slow motion); vector map produced using 0.1 relaxation, 5 iterations. Right: an adequate number of iterations fills in the measurement gaps; vector map produced using 0.1 relaxation, 40 iterations.

SMART Iterations: Voxel reconstruction is an iterative procedure, with the required number of iterations dependent on the relaxation parameter and how noisy a given dataset is. For the described four-camera setup with the 5:1 volumetric illu-

mination optics, resulting in an illumination depth of approximately 50 mm and a strong signal-to-noise ratio, 2 iterations were found to produce satisfactory results for relaxation numbers even as low as 0.001 (Figure A.1, left). When the illumination optics were further expanded to cover an illumination depth of nearly 100 mm, the signal-to-noise ratio was approximately half the signal-to-noise ratio of the 50 mm illumination depth. The lower signal-to-noise ratio for that image set necessitated an increase in SMART iterations, with 30 iterations at 0.2 relaxation found to be optimal.

Figures in Appendix A further illustrate the interaction between number of SMART iterations, relaxation number, and signal-to-noise ratio. As previously noted, datasets with strong signal-to-noise ratios and sharply defined particles are able to produce satisfactory measurement results using very small relaxation numbers and few iterations (Figure A.1). Small relaxation numbers appear to produce more accurate results than larger relaxation numbers, presumably due to larger relaxation numbers allowing more flexible determination of particle locations during voxel reconstruction. This may allow the formation of a greater number of ghost particles (see Wieneke [16] for further information on ghost particles), leading to larger inaccuracies in measurement results. Figures A.3, A.4, and A.5 show differences in measurement results caused by increasing relaxation number. All three figures utilize analysis parameters identical to those used for Figure A.1 (left) (calculated using 0.001 relaxation), but with relaxation numbers increased to 0.01, 0.1, and 0.95, respectively. As relaxation number increases, the number of large, obviously incorrect velocity vectors also increases. The right-hand side of each figure displays the differences between the respective vector map and the vector map given in Figure A.1, with the magnitude of difference between vector maps increasing as the difference in relaxation number increases. Since the 0.001 relaxation vector map from Figure A.1 displays none of the characteristically observed signs indicating too few SMART iterations were used for

a given relaxation number, it can be assumed that SMART reconstruction is able to perform accurate reconstructions using few iterations even at low relaxation numbers, provided the dataset has a strong signal-to-noise ratio and clearly defined particles. Under these conditions, SMART reconstruction can quickly identify true particle locations, and the general rule that small relaxation numbers require more iterations is irrelevant since the initial measurement results are already adequate with few iterations. Thus, it is more accurate to state that low relaxation numbers require more iterations to show improvement of results, not that low relaxation numbers necessarily require more iterations to produce good results.

Figure A.1 has shown that it is possible to use few iterations to produce acceptable results even with very low relaxation numbers, but this is predicated on having a dataset with a strong signal-to-noise ratio. For datasets with weak signal-to-noise ratios, larger relaxation numbers are required to complete TomoPIV analysis in a reasonable amount of time. The measurement results in Figure A.2, calculated from a dataset with a weak-signal-to-noise ratio, quite clearly show the characteristic measurement gaps associated with running too few SMART iterations for a given relaxation number. Even when the iterations are increased from 5 to 40, there is a negligible improvement in results. At very low relaxation numbers, results obviously cannot be improved without increasing iterations to an unreasonably large number, and in fact DynamicStudio currently limits the maximum number of SMART iterations to 100. Consequently, the relaxation number must be increased in order to improve measurement results. Even though low relaxation numbers were observed to produce the smoothest and most accurate vector maps with the fewest irrationally large vectors, noisy datasets contain too great of uncertainty in particle location to allow for the use of very small relaxation numbers. Low relaxation numbers allow minimal leeway when determining particle locations during voxel reconstruction, so using small relaxation numbers on datasets with large particle location uncertainty

will cause many particle locations to be rejected as false, unless very large numbers of iterations are allowed. The strength and clarity of the measurement signals can therefore be said to have the greatest impact on optimal relaxation number and required number of SMART iterations. Noisy data requires larger relaxation numbers and more iterations, while strong signal-to-noise ratios allow for low relaxation numbers and few iterations.

3.3 3D LEAST SQUARES MATCHING

DynamicStudio's 3D Least Squares Matching technique produces velocity vector maps based on changes in particle locations between two temporally sequential voxel spaces. This section will describe various settings that affect LSM results. This section will also provide examples indicating poor results and the actions that will likely improve those results.

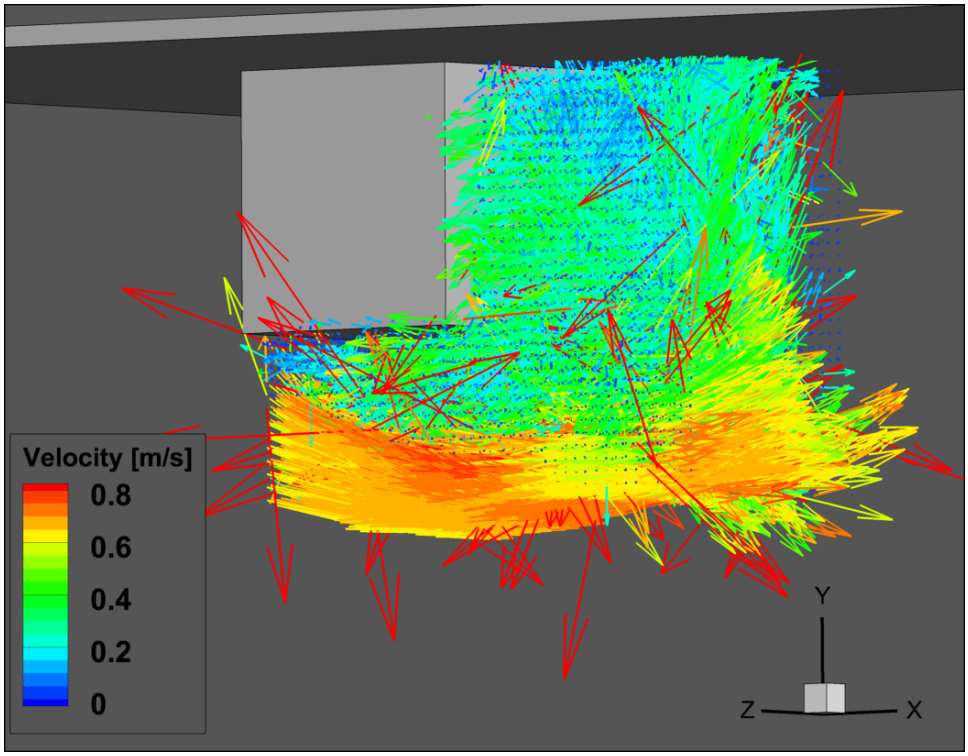

Figure 3.6: Vector map created using an insufficiently large IV size, producing noisy measurement results (used IV size of 51x51x51 voxels; recommended minimum IV size was 71x71x71 voxels).

The LSM technique calculates velocity vectors based on particle motion observed in groups of voxels referred to as Interrogation Volumes (IV). The DynamicStudio manual [15] specifies that a minimum of 8 to 9 particles should be present per IV in order for LSM to perform well. The minimum required IV size can therefore be estimated based on the seeding density observed in the measurement images. The DynamicStudio manual provides a chart to assist with determining appropriate IV size based on seeding density and measurement depth. Insufficient IV size for a given seeding density produces a relatively rough and inconsistent vector map, as seen in Figure 3.6. The vector map in Figure 3.6 was produced using an IV size of 51 x 51 x 51 voxels, while the recommended minimum IV size was roughly 71 x 71 x 71 voxels. Increasing the IV size produces smoother vector maps since there are more particles present in each IV. Having more particles helps mitigate inaccuracies stemming from incorrect particle identification during voxel reconstruction. The difference in accuracy and smoothness can be observed when comparing Figure 3.6 (51 x 51 x 51 voxel IV) with Figure 3.7 (75 x 75 x 75 voxel IV), both of which were calculated from the same voxel space with a recommended minimum IV size of roughly 71 x 71 x 71 voxels.

One other parameter that has a potentially significant impact on LSM results is the time step between image frames. An instructional presentation from Dantec Dynamics [17] recommends using a time step that results in a maximum particle displacement between frames of roughly 1/4 of the IV size. When selecting a time step, one should take into account both the slowest- and fastest-moving portions of the measurement region of interest. Particle displacement in the fastest potions should not significantly exceed the recommended 1/4 IV size limit, while the slowest portions should exhibit at least a minimum of discernible motion, greater than 1 or 2 pixels. Note that the measurement region of interest (e.g. a turbulent wake region) may be surrounded by a fast-moving free stream region. In instances such as this, the free

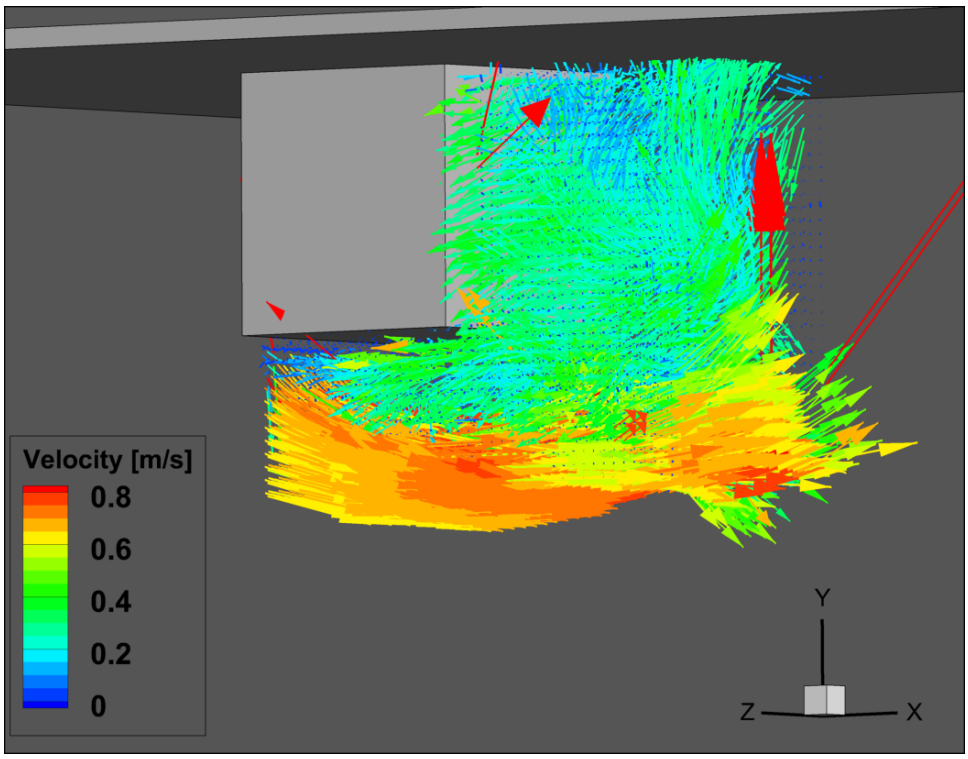

Figure 3.7: Vector map created using a sufficiently large IV size, producing relatively smooth measurement results (used IV size of 75x75x75 voxels; recommended minimum IV size was 71x71x71 voxels).

stream region is likely not of great interest, and can be ignored when determining an appropriate measurement time step. Additionally, regions of laminar flow typically produce reliable measurement results even for particle displacements exceeding the recommended 1/4 IV size limit because of the simplicity of the flow regime.

For the described experimental setup, the LSM technique produced unexpected results when particles displacements were very small. Figure 3.8 displays LSM measurement results (range-validated and spatially averaged for clarity) based on very small particle displacements (1 to 2 pixels). The measurement volume was calibrated to a depth of 100 mm, but with an illumination depth of only the central 50 mm. The maximum possible depth over which velocity vectors can be calculated is roughly the calibration depth minus twice the IV size. For the measurement in Figure 3.8 this was roughly 75 mm. Theoretically, velocity vectors should only be calculated

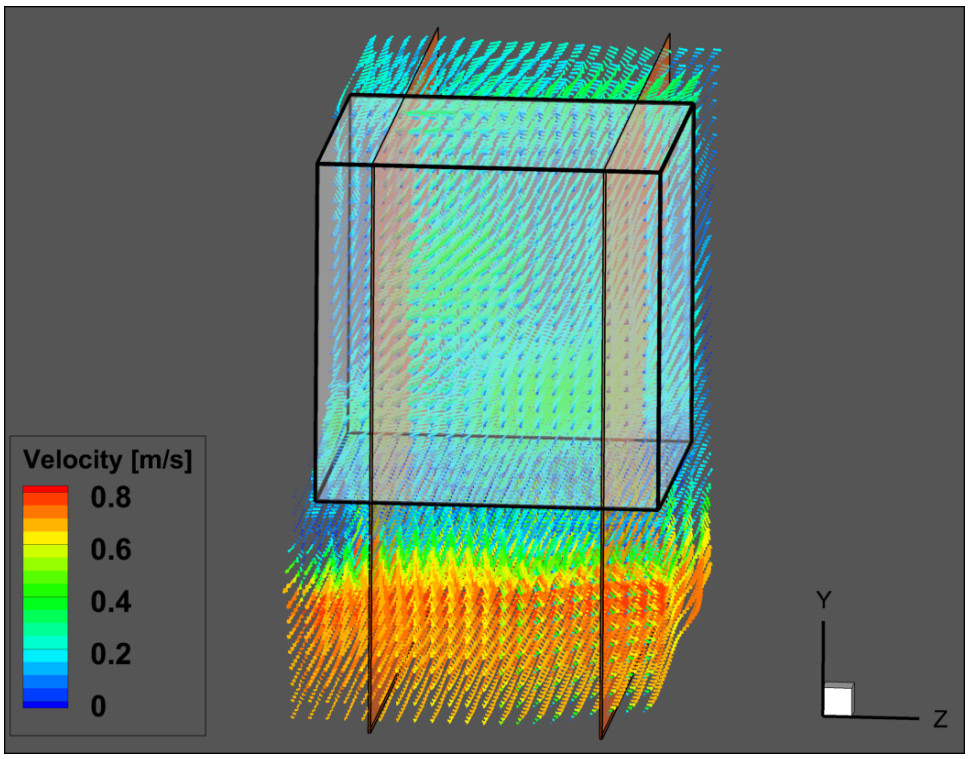

Figure 3.8: LSM measurement results based on an insufficiently large time step (resultant particle displacements of 1 to 2 pixels). Velocity vectors extend beyond 50 mm illumination depth (region between planes).

across the illuminated depth, with the regions outside the illumination showing no visible particles, and therefore no motion. The time step for this measurement, 1100 μs, was too short to give adequately large particle displacements in the wake region behind the 75 mm model cube, resulting in displacements of only 1 to 2 pixels (equivalent to roughly one particle width in this experimental setup). When particle displacements are too small, the LSM technique has been observed to produce velocity vectors across the entire allowable measurement depth, not just the 50 mm that was actually illuminated. For comparison, Figure 3.9 was created based on a time step of 2500 μs, which resulted in wake region particle displacements of roughly 5 to 6 pixels. The LSM results showed a more reasonable arrangement of vectors in Figure 3.9 (also range-validated and spatially averaged for clarity), with vectors roughly confined to the illuminated central 50 mm region. Note also, however, that the vectors

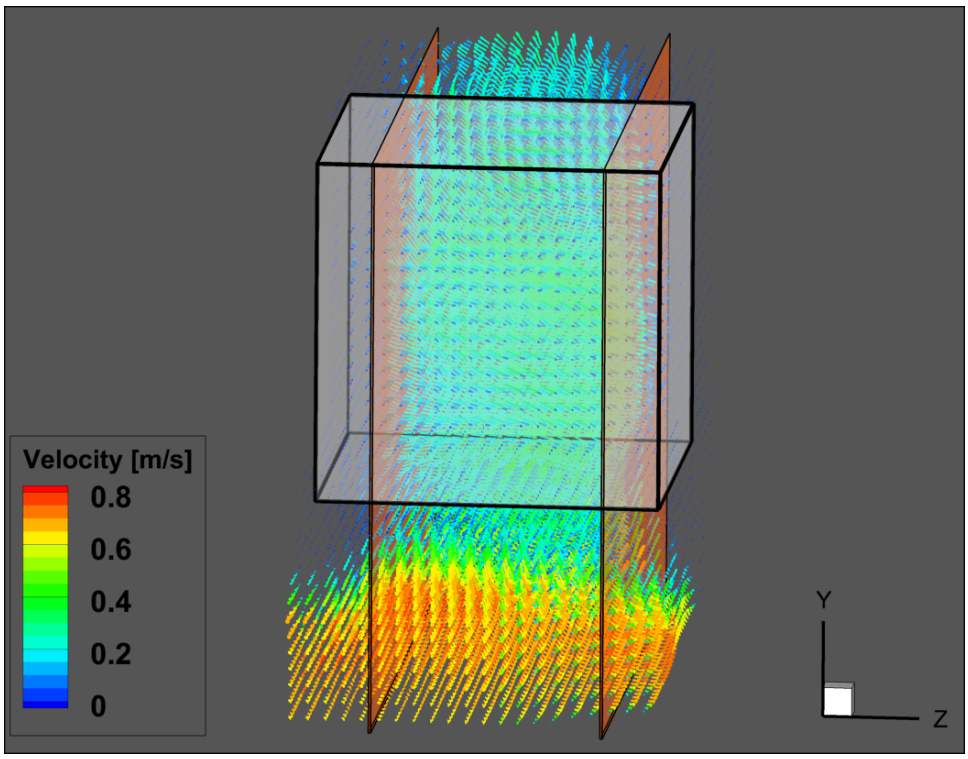

Figure 3.9: LSM measurement results based on a sufficiently large time step (resultant particle displacements of 5 to 6 pixels). Velocity vectors generally confined to 50 mm illumination depth (region between planes).

representing the free-stream region below the model cube generally extend across the entire allowable measurement depth despite having even larger particle displacements than the wake region, averaging roughly 15 pixels. Further measurement runs indicate that the LSM technique produces this extended depth of vectors for regions of uniform flow, such as the free stream region, regardless of particle displacement value.

Additionally, use of the custom filter during image pre-processing appears to reduce the extent or severity of the problems associated with insufficient particle displacements. As noted in Section 3.1, when the custom filter is not applied during pre-processing (instead replaced by careful thresholding), the extended vector depth issue occurred at larger time steps. When images were pre-processed using the custom filter, the 2500 μs time step appeared to be sufficiently large and showed a very limited number of vectors extending beyond the illuminated depth (Figure 3.9). When

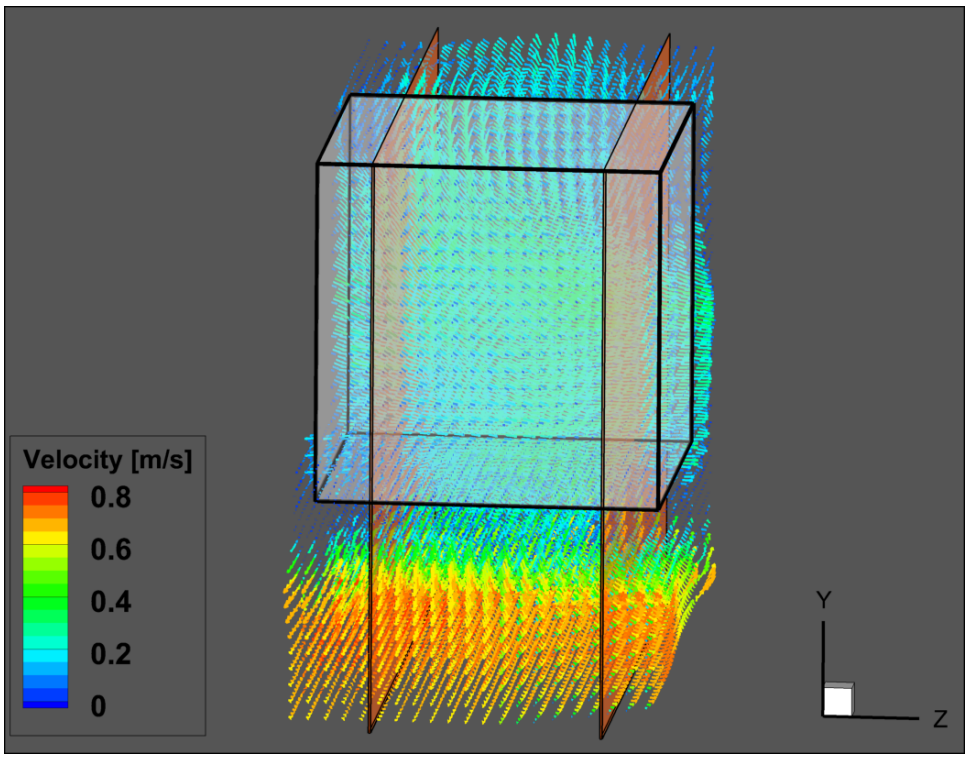

Figure 3.10: LSM measurement results based on the same time step as Figure 3.9. Image pre-processing utilized only thresholding, no custom filter. Vectors once again extend beyond 50 mm illumination depth (region between planes).

thresholding is applied instead of the custom filter, the 2500 μs time step (Figure 3.10) no longer appeared to be sufficiently large, with many vectors extending beyond the illumination depth. This indicates that the overall vector depth extension issue may relate to the amount of noise remaining in the processed images, and by extension the number of ghost particles created during voxel reconstruction.

Ghost particles may be formed at locations where the line of sight from all four cameras coincides with an observed particle location, but the observed particle is not the same for all four cameras. This may be due to overlapping particles, or from noise being treated as a possible particle in one or more cameras. At small time steps the particles move very little between frames, so any conditions that caused the formation of a ghost particle in the first frame may still exist in the second frame. This would create a ghost particle in the second frame that is shifted very slightly

from the location of the ghost particle in the first frame. Since this shift stems from the motion of true particles, the LSM algorithm will likely be able calculate a satisfactory correlation for the movement of all ghost particles. These ghost particles may be formed outside the illuminated volume, which would result in motion vectors outside the illuminated region that appear consistent with the motion observed within the illuminated region. At larger time steps, the particles shift a greater amount. The shift may eliminate the conditions that caused the formation of a ghost particle in the first frame, so there would not be a matching ghost particle created in the second frame. The LSM algorithm would therefore be unable to find consistent correlations for ghost particle motion outside the illuminated region for larger time steps.

If, however, there is sufficient noise in an image set, pairs of ghost particles may still be formed at larger time steps. When purely using thresholding and not the custom filter (as was the case in Figure 3.10), there are many instances where small groups of background pixels remain untouched after the threshold is performed. Despite the increased particle shift between frames, that extra noise increases the chance that both frames will contain conditions that allow the formation of ghost particles that mimic the motion of true particles. This would explain the presence of vectors outside the illuminated region in Figure 3.10.

3.4 EFFECTS OF REFLECTION MITIGATION

Reflection mitigation techniques are important during TomoPIV measurements when a physical model is placed inside the illuminated volume. Surface reflections from the model can increase background noise in images and potentially cause unwanted illumination of particles outside the calibrated measurement volume. Various reflection mitigation techniques are known and discussed [6, 7, 8, 9], but how the reflection mitigation techniques, or lack there-of, affect PIV measurement results is generally unexplored. This section describes the observed differences in measurement results of a four-camera TomoPIV system, as detailed in Bisel et al. [1].

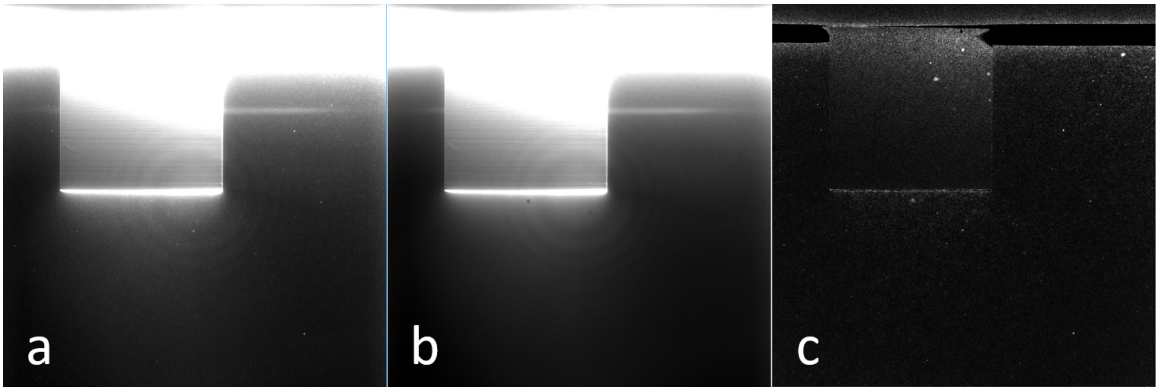

Figure 3.11: Background subtraction sequence for camera 1 (centerline) view of white model: raw image (a), image min (b), background subtraction (c).

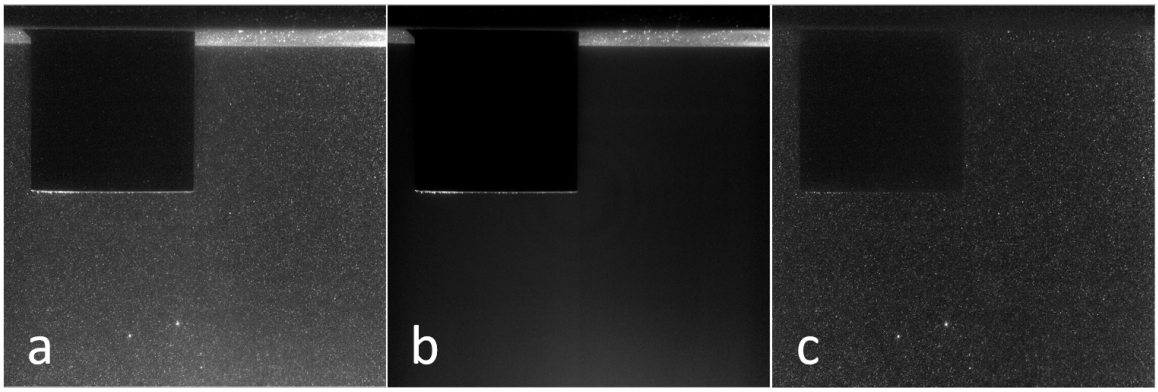

Figure 3.12: Background subtraction sequence for camera 1 (centerline) view of Rhodamine 6G model: raw image (a), image min (b), background subtraction (c).

Separate measurement runs were conducted with a cubic bluff body model coated with Rhodamine 6G fluorescent paint and flat white aerosol paint. In conjunction with a narrow band-pass optical filter, the Rhodamine 6G paint reduced surface reflections to negligible levels, while the flat white paint provided no reflection mitigation. The effects of two different types of surface reflections are observed: direct and indirect reflections. As described in Bisel et al.: "direct reflection is defined as light that is reflected off a surface that is within a camera's direct line of sight. Indirect reflection is defined as light that is reflected off a surface that cannot be seen directly by a camera. The indirectly reflected light only becomes visible to the camera after it is

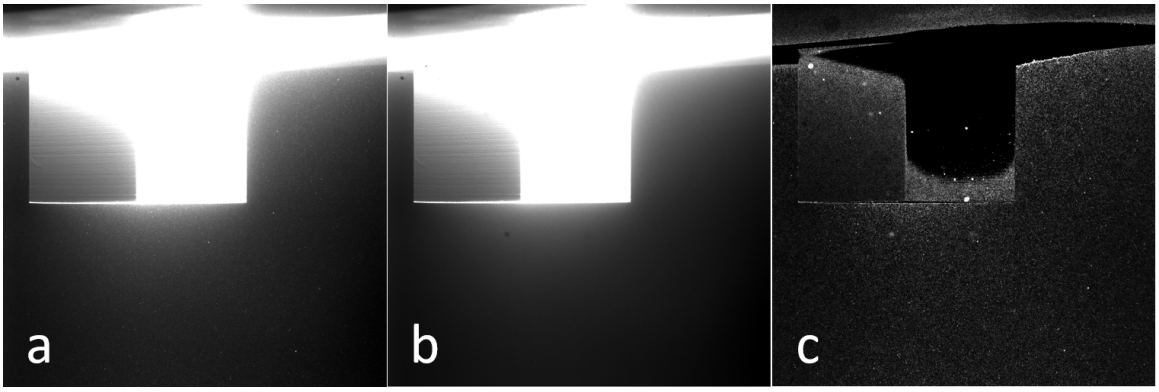

Figure 3.13: Background subtraction sequence for camera 4 (45 degree offset) view of white model: raw image (a), image min (b), background subtraction (c).

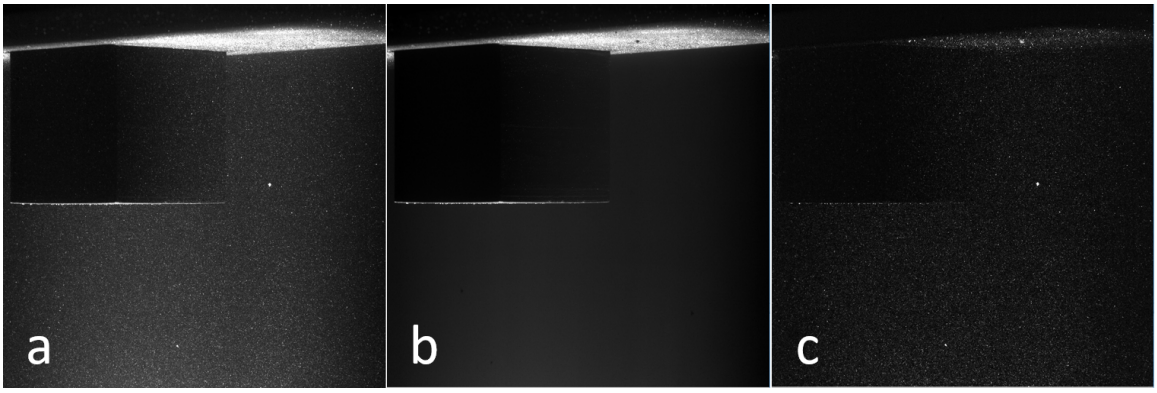

Figure 3.14: Background subtraction sequence for camera 4 (45 degree offset) view of Rhodamine 6G model: raw image (a), image min (b), background subtraction (c).

scattered by surrounding particulate matter."

The white model showed marginally higher average seeding density than the Rhodamine 6G model, since the strong indirect reflections from the model surfaces added a second pass of illumination to the particles. This is notably visible in Figure 3.11a where the particles directly below the model surfaces are brighter than particles in surrounding regions. Comparatively, in Figure 3.12a the particle brightness is uniform across the entire image and gains no additional illumination from surface reflections. However, the background noise is much higher for the white model. The image minimum calculated during background subtraction is representative of the background

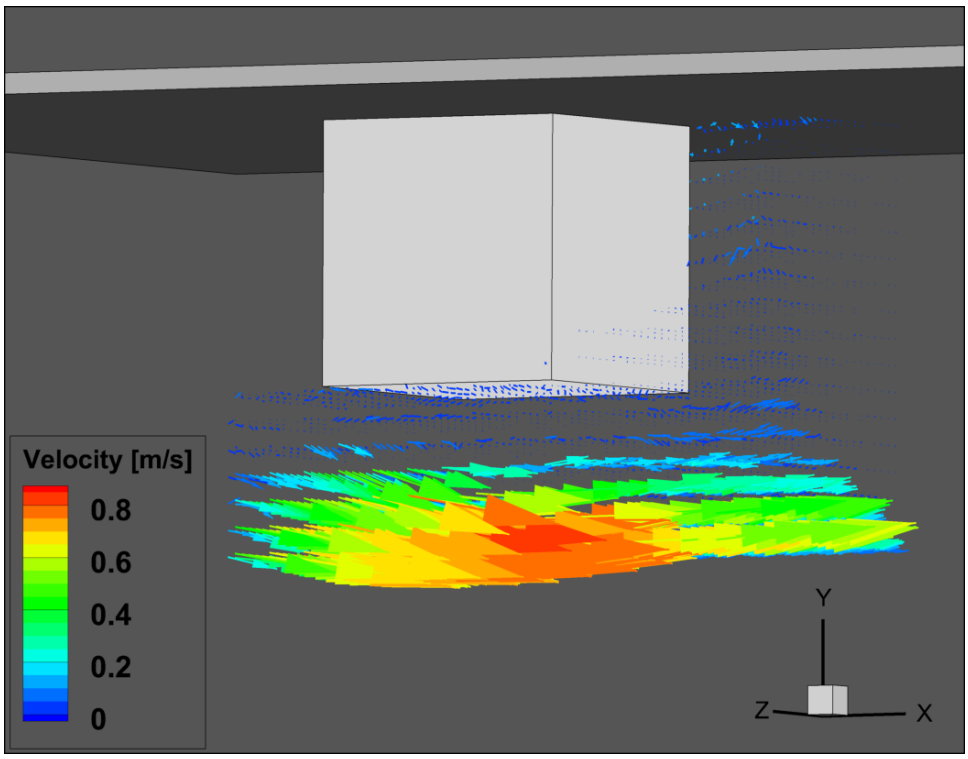

Figure 3.15: Average of 125 vector maps for the white paint model (angled front view).

noise present in an image set. Based on the pixel gray values for the white and Rhodamine 6G model image minimums (Figures 3.11b and 3.12b), the region directly below the white model shows 65 times greater background noise than the same region for the Rhodamine 6G model. The high intensity background noise in the region below the model for the flat white images means that the signal-to-noise ratio is significantly worse than that of the Rhodamine 6G paint images. The signal-to-noise ratio for the region directly below the model was approximately 10 for the brightest particles in the Rhodamine 6G paint images and approximately 2 for the brightest particles in the white paint images. This is despite the fact that the particles in the flat white images are typically an order of magnitude brighter than the particles in the Rhodamine 6G images.

Figures 3.11c and 3.12c show the flat white and Rhodamine 6G models after using

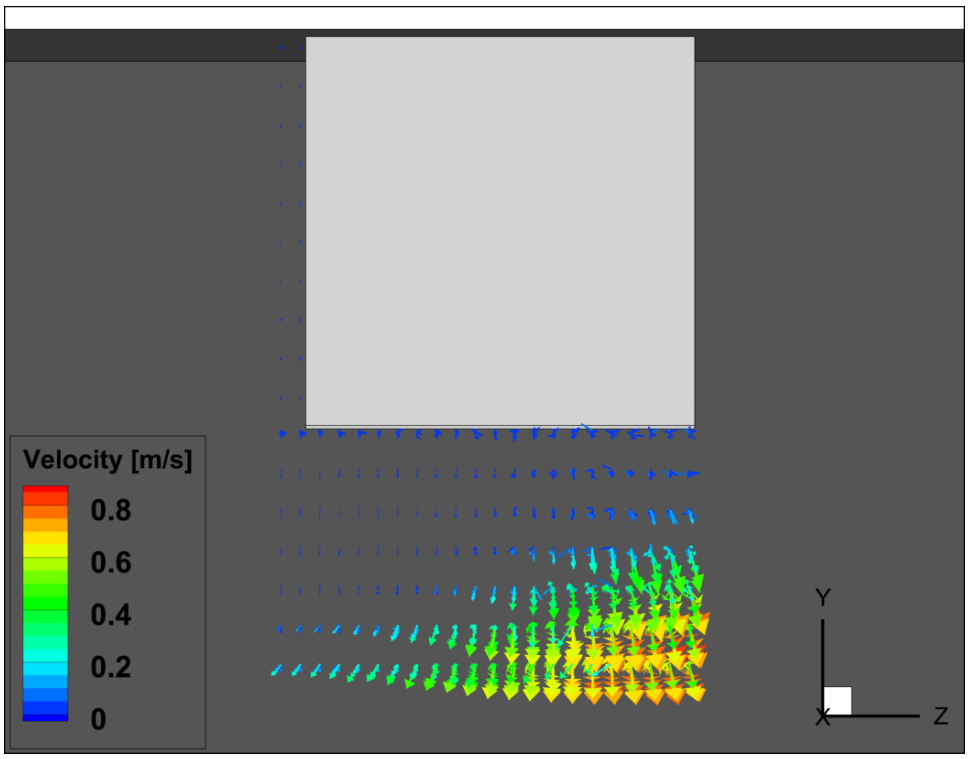

Figure 3.16: Average of 125 vector maps for the white paint model (upstream view).

a background subtraction to reduce the amount of noise in the images. The background subtraction removed a significant portion of the white image brightness. In the region below the white model, typical particles lost between 80% and 90% of their intensity. Typical particles in the region below the Rhodamine 6G model lost only approximately 10% of their intensity since the Rhodamine 6G paint greatly mitigates the background noise stemming from indirect surface reflections.

Particles that are distant from the cameras have lower intensities than particles close to the cameras. Intense background noise, such as that seen in the region below the white model in Figure 3.11a, can make it very difficult to differentiate between background noise and distant particles. A background subtraction is used to improve signal-to-noise ratios, but if the background noise intensity is close to the intensity of distant particles, the background subtraction may remove a significant portion of a distant particle's intensity. In that case, the background subtraction will

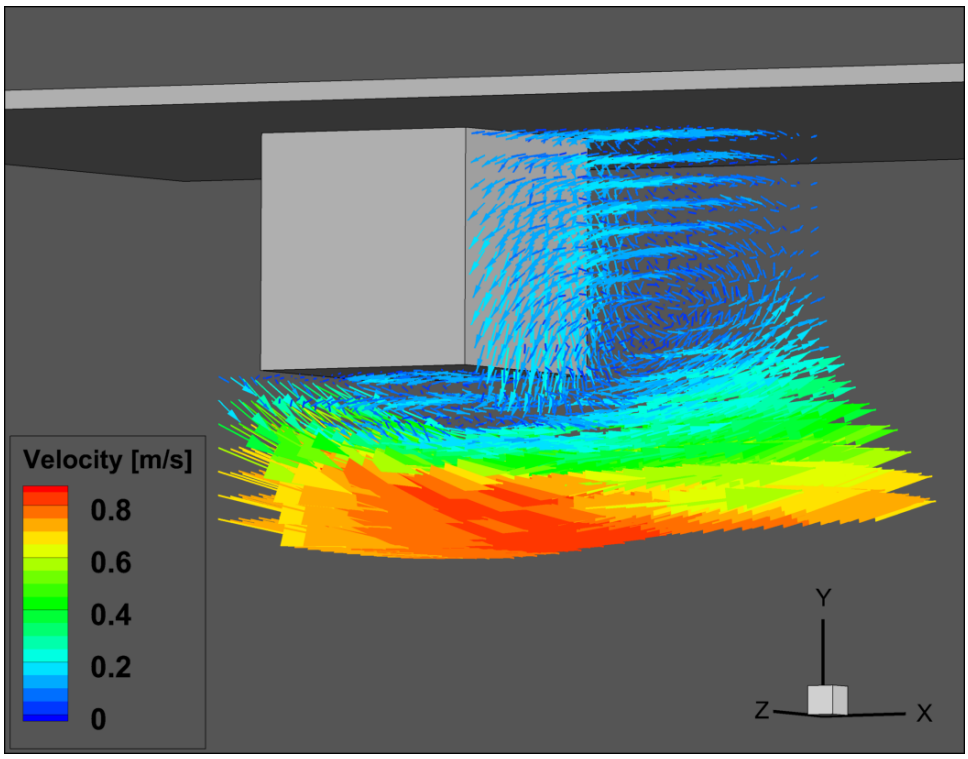

Figure 3.17: Average of 125 vector maps for the Rhodamine 6G paint model (angled front view).

not significantly improve the signal-to-noise ratio of distant particles, which makes particle recognition difficult during voxel reconstruction.

Direct reflections can be much brighter than indirect reflections. The direct reflections stemming from the white model's rear face and the flat mounting plate (Figure 3.13a) have high enough intensity to completely saturate the camera pixels. Since the pixels in this region are all at the camera's maximum allowed intensity, there is no contrast in the region, giving a signal-to-noise ratio of exactly 1. No particles can be distinguished in this region, which can be more easily seen after a background subtraction is performed in Figure 3.13c. All pixels across all doubleframes in the image set have the same value in this region, so the background subtraction removes all intensity and leaves a uniformly black region. Direct reflections are greatly mitigated for the Rhodamine 6G model, as seen in Figure 3.14a. After a background subtrac-

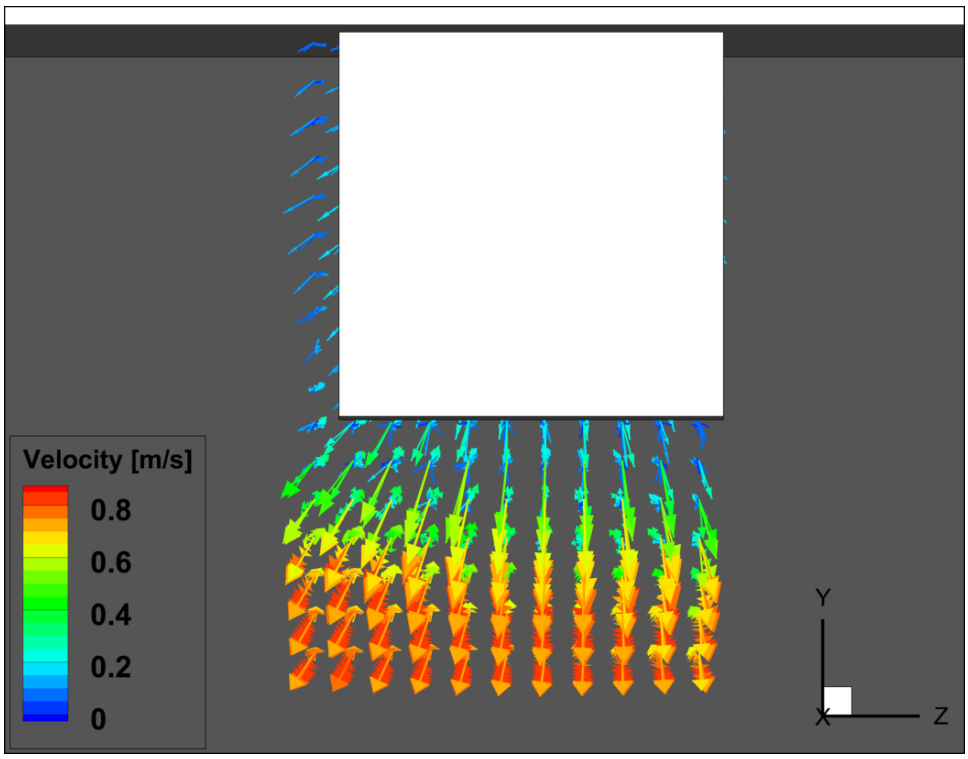

Figure 3.18: Average of 125 vector maps for the Rhodamine 6G paint model (upstream view).

tion is performed (Figure 3.14c) the effects of any direct reflections are negligible, ensuring that particle recognition is easily achievable during voxel reconstruction.

A comparison of vector flow maps for the flat white and Rhodamine 6G models illustrates the need for reflection mitigation techniques for TomoPIV analysis. The displayed vector maps were created by averaging the 125 vector maps calculated from the respective white and Rhodamine 6G measurement runs. Figure 3.15 confirms expectations that no measurements can be made in regions of intense direct reflections since no particles are distinguishable. It is still possible to make measurements in the regions where there are no intense direct reflections, such as the free-stream region, but with some limitations. Figure 3.16 shows that intense indirect reflections limit the distance at which measurements can be accurately made. Intense indirect reflections interfere with recognition of distant particles. The allowable measurement depth is

therefore limited by the intensity of the indirect reflections.

Figures 3.17 and 3.18 demonstrate the capability of TomoPIV analysis when employing effective reflection mitigation. Measurements appear uniformly accurate across the entire measurement depth, indicating that indirect reflections from the Rhodamine 6G model are negligible and thus do not limit measurement depth. Direct reflections from the rear face of the model are also negligible and have no impact on particle recognition capability.

CHAPTER 4: CONCLUSIONS

This thesis highlights techniques and methodologies useful for conducting TomoPIV measurements, and also explains ways in which TomoPIV analysis settings influence measurement results. Observations are made based on an asymmetric four-camera TomoPIV system's measurement results based on seed particles suspended in water.

Image pre-processing is necessary to complete TomoPIV measurements in a reasonable time frame and reduce computer memory requirements during voxel reconstruction. This is especially important for large voxel spaces, where available computer memory may be a limiting factor. The purpose and effects of several pre-processing techniques are described.

A background subtraction is useful to enhance signal-to-noise ratios by removing static noise from images. A custom filter (Figure 3.4) has proven to be simple to implement and useful for reducing memory requirements during voxel reconstruction. The custom filter effectively concentrates surrounding pixel light intensities into particle locations. Particle brightness is enhanced, and surrounding pixel gray values are reduced to zero, typically removing roughly 3/4 of all pixel intensities. This greatly reduces voxel reconstruction memory requirements and improves reconstruction speed. Thresholding can further increase reconstruction speed by removing any low-level pixel gray values remaining after the custom filter is applied.

Parameters affecting the results of SMART voxel reconstruction are explored. Voxel reconstruction is an iterative procedure, with the required number of iterations dependent on measurement signal strength and relaxation number. Weak measurement signals and smaller relaxation numbers may require more iterations. For all tested measurements utilizing relaxation numbers ranging from 0.001 to 0.95, signal strength

appears to be the dominant factor for determining required number of iterations, with high signal strengths requiring few iterations even for low relaxation numbers (2 iterations found acceptable even for relaxation numbers as low as 0.001). Low relaxation numbers do not necessarily require large numbers of iterations to achieve acceptable results. Instead, low relaxation numbers require large numbers of iterations to show improvement of poor results. Gaps in measurement data are indicative of running too few SMART iterations for a given relaxation number. The measurement gaps can be observed as spaces where no vectors are visible in LSM vector maps. The measurement gaps can be filled in by increasing the number of SMART iterations, with lower relaxation numbers requiring more iterations to fill in the gaps.

The quality of 3D LSM vector maps is dependent on the IV size used during calculation. The minimum required IV size is determined from the seeding density of the measurement images, with lower seeding densities requiring large IV size to encompass an adequate number of particles (8-9) per IV [15]. Inadequate IV sizes produce noisy vector maps, while larger IV sizes produce smoother vector maps. The 3D LSM technique may produce misleading vector maps if image frames are not separated by a time step large enough to allow sufficient particle motion between frames. In instances where the calibrated measurement depth is larger than the illumination depth and the time step between measurement frames results in particle displacements of less than one particle width (e.g. 1 to 2 pixel displacements relative to particle widths of 2 to 3 pixels), the 3D LSM technique is observed to produce vector maps displaying consistent motion over the entire calibrated depth even though particle motion should only be visible inside the illumination volume.

Reflection mitigation techniques are required for TomoPIV measurements when a physical model must be placed within the illumination volume. The impact of surface reflections on TomoPIV measurements is examined using a four-camera TomoPIV system to conduct measurements involving a cubic bluff body coated first

with a commercially available flat white aerosol paint, and second with an airbrushed Rhodamine 6G fluorescent paint. The Rhodamine 6G fluorescent paint, coupled with optical bandpass filters to block the fluoresced light, reduces surface reflections to negligible levels. Flat white paint affords no reflection mitigation capability, and thus produces high intensity surface reflections. High intensity reflections from model surfaces prevent any possible TomoPIV measurements in the image regions for which those surfaces are directly visible. The high intensity reflections completely saturate the pixels in those image regions, preventing particle recognition during TomoPIV analysis. Reflections from the underside of the white painted bluff body, despite not being directly visible to any camera, also interfere with TomoPIV measurements by increasing the background noise intensity of the region below the bluff body. The increased noise interferes with particle visibility in the rear of the measurement volume (the region located furthest from the cameras). Particles closer to the cameras are generally bright enough to remain visible despite the increased background noise. TomoPIV measurements for the volume beneath the bluff body are therefore still possible in the regions closest to the cameras, while becoming more unreliable as distance increases from the cameras and particle visibility degrades.

Measurements of the Rhodamine 6G bluff body show consistent measurement reliability across the entire measurement depth. This is due to the low intensity surface reflections that result in low background noise intensity. Comparing the Rhodamine 6G and white paint TomoPIV measurement results indicates that allowable measurement depth decreases as surface reflection intensity increases. Effective reflection mitigation techniques are therefore crucial to the success of TomoPIV analysis of large measurement depths.

Depending on factors such as size of voxel space and desired vector map resolution, TomoPIV measurements can be extremely computationally intensive. Extensive trial-and-error attempts at improving measurement results can therefore be time-

prohibitive. The techniques and observations presented in this thesis should serve as a guide for improving data acquisition and processing methodologies, recognizing potential measurement errors, and optimizing analysis settings and measurement results, with the goal of making TomoPIV methodologies more accessible to those unfamiliar with this form of measurement system.

REFERENCES

[1] T. T. Bisel, J. L. Dahlberg, T. R. Martin, S. S. Owen, R. G. Keanini, P. T. Tkacik, N. Narayan, and N. Goudarzi, "A comparison of flat white aerosol and rhodamine (r6g) fluorescent paints and their effect on the results of tomographic piv measurements," in *Procedings of the ASME 2017 International Mechanical Engineering Congress and Exposition*, 2017.

[2] R. J. Adrian, "Scattering particle characteristics and their effect on pulsed laser measurements of fluid flow: speckle velocimetry vs particle image velocimetry," *Applied optics*, vol. 23, no. 11, pp. 1690–1691, 1984.

[3] R. J. Adrian, "Twenty years of particle image velocimetry," *Experiments in fluids*, vol. 39, no. 2, pp. 159–169, 2005.

[4] G. E. Elsinga, F. Scarano, B. Wieneke, and B. W. van Oudheusden, "Tomographic particle image velocimetry," *Experiments in Fluids*, vol. 41, no. 6, pp. 933–947, 2006.

[5] F. Scarano, "Tomographic piv: principles and practice," *Measurement science and technology*, vol. 24, no. 1, 2012.

[6] E. Paterna, P. Moonen, V. Dorer, and J. Carmeliet, "Mitigation of surface reflection in piv measurements," *Measurement science and technology*, vol. 24, no. 5, p. 057003, 2013.

[7] F. J. Martins, J.-M. Foucaut, L. F. Azevedo, and M. Stanislas, "Near-wall study of a turbulent boundary layer using high-speed tomo-piv," in *Progress in Wall Turbulence 2*, pp. 347–356, Springer, 2016.

[8] R. Konrath, C. Klein, A. Schröder, and J. Kompenhans, "Combined application of pressure sensitive paint and particle image velocimetry to the flow above a delta wing," *Experiments in Fluids*, vol. 44, no. 3, pp. 357–366, 2008.

[9] J. M. Edwards, L. A. Danao, and R. J. Howell, "Piv measurements and cfd simulation of the performance and flow physics and of a small-scale vertical axis wind turbine," *Wind Energy*, vol. 18, no. 2, pp. 201–217, 2015.

[10] P. M. Danehy, P. I. Tiemsin, C. J. Wohl, M. Verkamp, T. Lowe, P. Maisto, G. Byun, and R. Simpson, "Fluorescence-doped particles for simultaneous temperature and velocity imaging," 2012.

[11] A. J. Pierce and F. K. Lu, "New seeding and surface treatment methods for particle image velocimetry," in *49th AIAA aerospace sciences meeting including the new horizons forum and aerospace exposition*, 2011.

[12] E. Fleischhauer, J. L. Dahlberg, T. T. Bisel, P. T. Tkacik, and S. Hellman, "Tomographic piv measurement in a bluff body wake utilizing an asymmetric camera configuration and least squares matching," in *55th AIAA Aerospace Sciences Meeting*, p. 1644, 2017.

[13] "R6g rhodamine fluorescent paint." Produced by Flow Visualization Components, dr.gindele-fischer-nauwerck GBR.

[14] "Strust +sspr 6pk flat white safety data sheet," May 2017. Rust-Oleum Corporation.

[15] Dantec Dynamics, *DynamicStudio User's Guide*, 2017.

[16] B. Wieneke, "Piv uncertainty quantification and beyond," December 2017.

[17] S. Hellman, "3d-capabilities / vv boundaries / planning a measurement." A Dantec Dynamics presentation, 2016.

APPENDIX A: VOXEL RECONSTRUCTION ITERATION AND RELAXATION COMPARISONS

The figures in this appendix further illustrate the impact of changing the relaxation parameter and the number of iterations used during SMART voxel reconstruction. Smaller relaxations require larger numbers of iterations to produce noticeable changes in results. Datasets with strong signal-to-noise ratios and sharply defined seed particles permit the use of smaller relaxation numbers and fewer numbers of iterations. Datasets with weak signal-to-noise ratios and poorly defined seed particles require larger relaxation numbers to produce reliable measurement results.

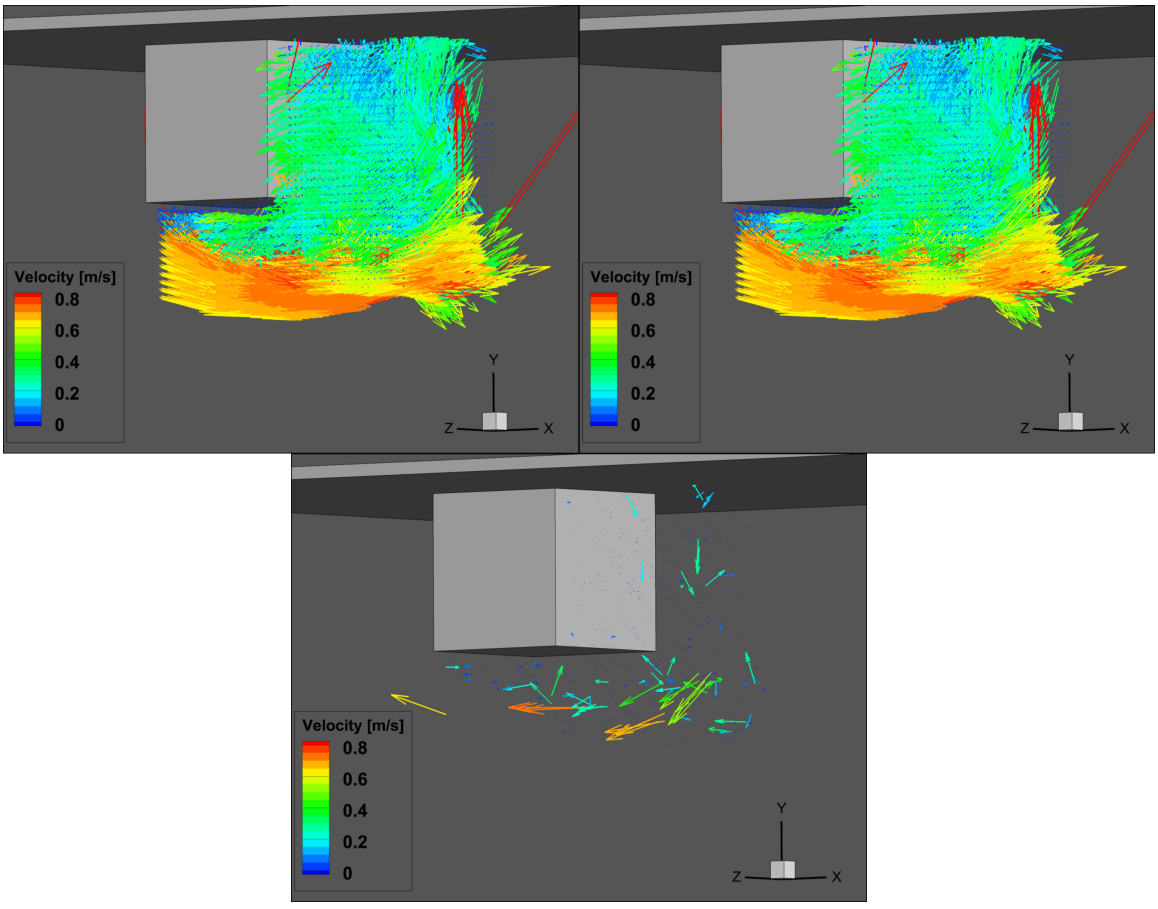

Figure A.1: Vector maps created using 0.001 relaxation from data with a strong signal-to-noise ratio. Left: 2 SMART iterations. Right: 30 SMART iterations. Bottom: Difference between results (left subtracted from right).

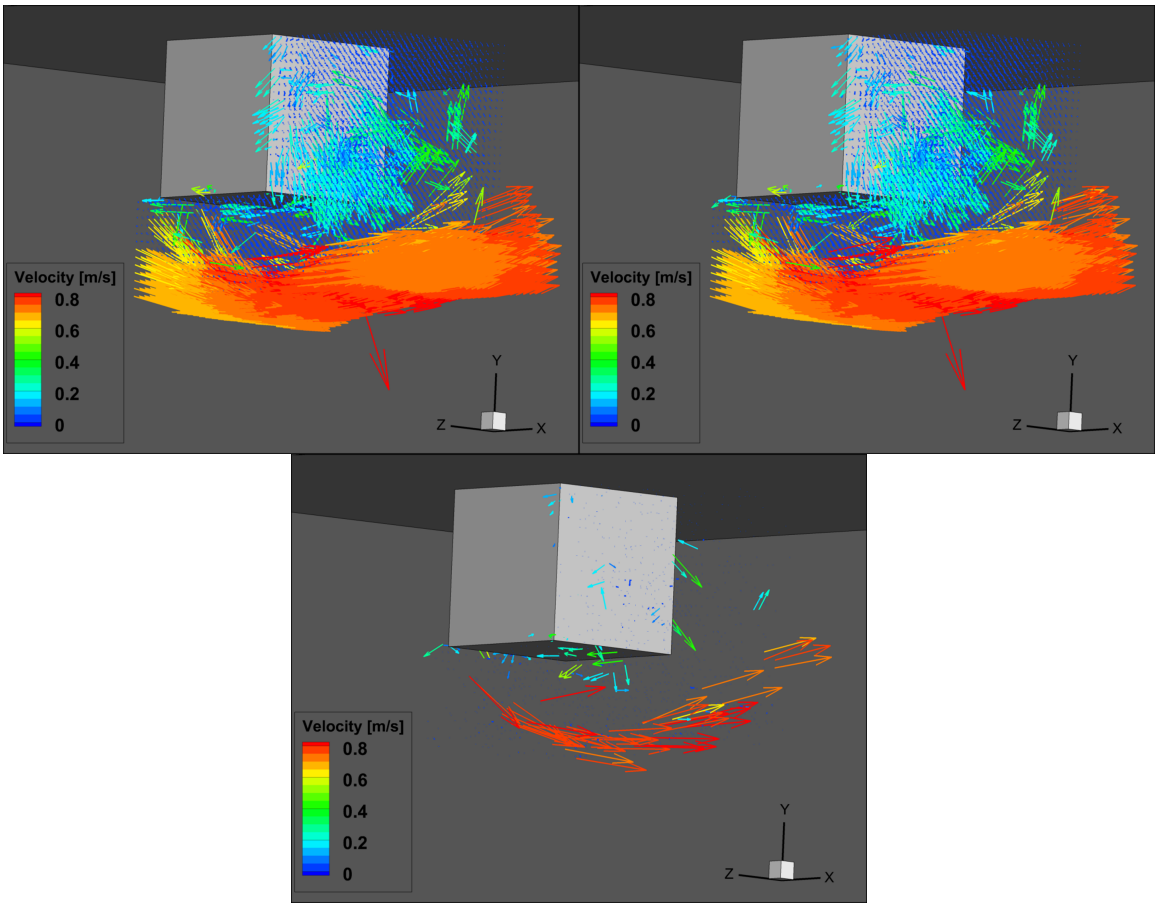

Figure A.2: Vector maps created using 0.001 relaxation from data with a relatively weak signal-to-noise ratio. Left: 5 SMART iterations. Right: 40 SMART iterations. Bottom: Difference between results (left subtracted from right).

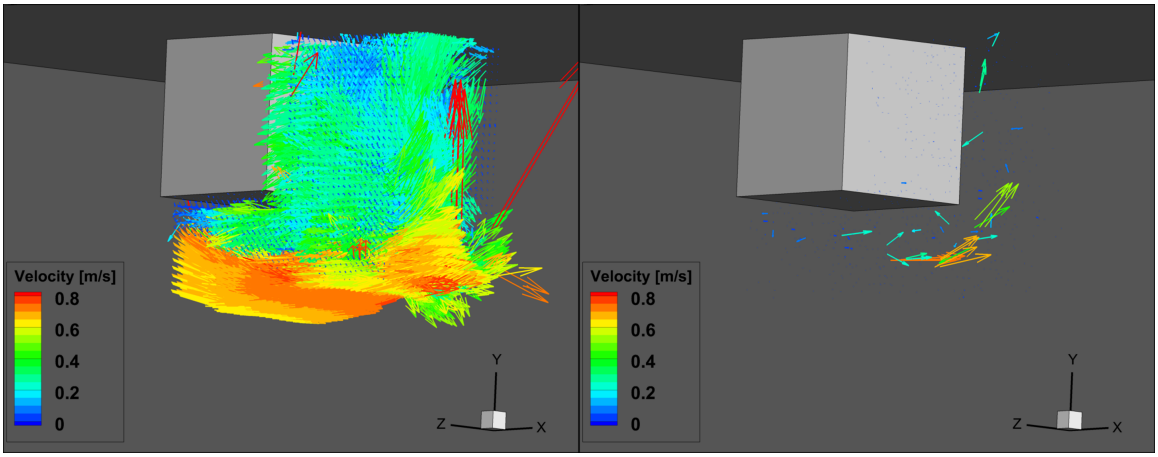

Figure A.3: Left: vector map created from the same data as Figure A.1 (0.001 relaxation), using 2 SMART iterations and 0.01 relaxation. Right: difference between 0.01 and 0.001 relaxation results.

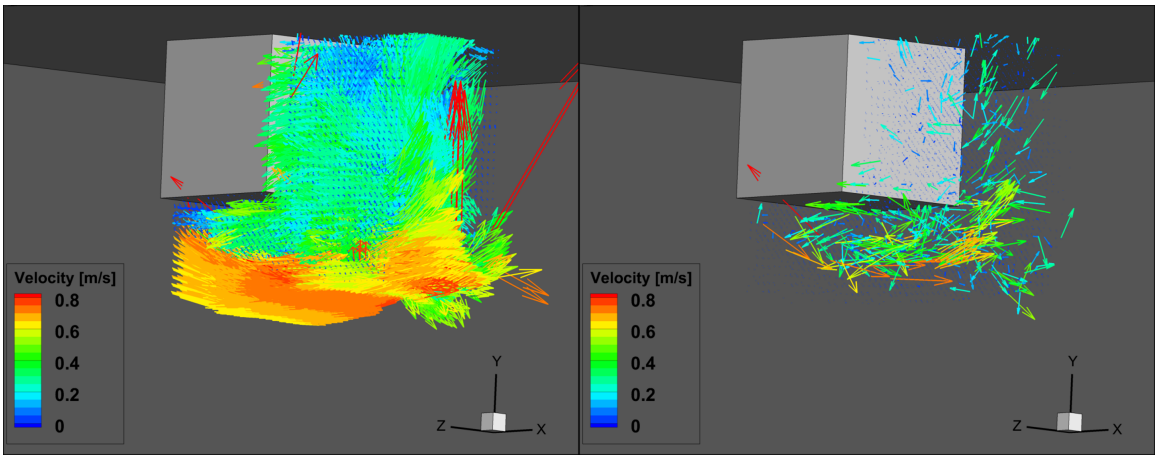

Figure A.4: Left: vector map created from the same data as Figure A.1 (0.001 relaxation), using 2 SMART iterations and 0.1 relaxation. Right: difference between 0.1 and 0.001 relaxation results.

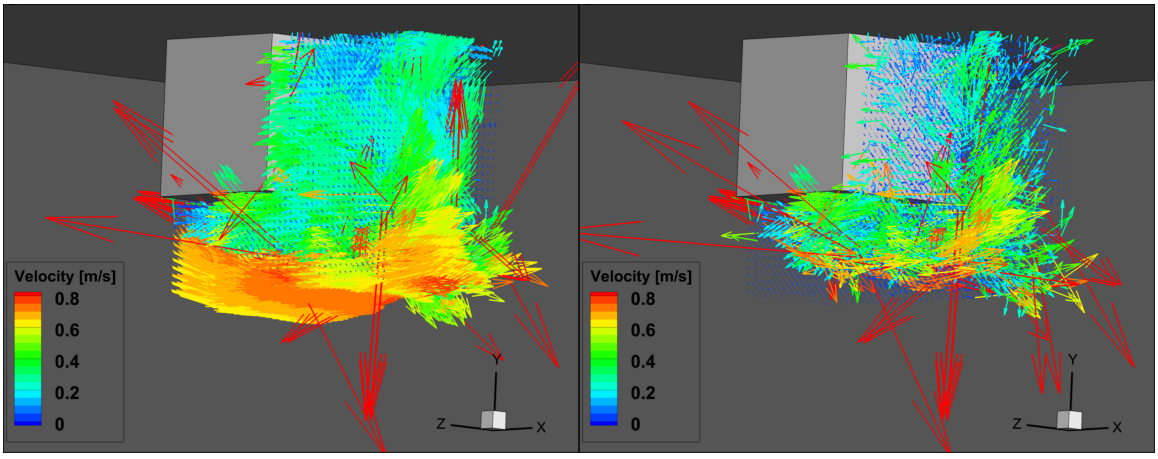

Figure A.5: Left: vector map created from the same data as Figure A.1 (0.001 relaxation), using 2 SMART iterations and 0.95 relaxation. Right: difference between 0.95 and 0.001 relaxation results.